BBA - Bioenergetics 1860 (2019) 271–285

Contents lists available at ScienceDirect

BBA - Bioenergetics

journal homepage: www.elsevier.com/locate/bbabio

Two-dimensional spectroscopy for non-specialists

Andrius Gelzinis[a,b], Ramūnas Augulis[b], Vytautas Butkus[a], Bruno Robert[c], Leonas Valkunas[a,b,*]

[a] Institute of Chemical Physics, Faculty of Physics, Vilnius University, Sauletekio 9-III, Vilnius 10222, Lithuania
[b] Department of Molecular Compound Physics, Center for Physical Sciences and Technology, Sauletekio 3, Vilnius 10257, Lithuania
[c] Institute for Integrative Biology of the Cell (I2BC), CEA, CNRS, Univ Paris-Sud, Université Paris-Saclay, F-91198 Gif-sur-Yvette cedex, France

ARTICLE INFO

Keywords:
Two-dimensional spectroscopy
Energy transfer
Pump-probe spectroscopy

ABSTRACT

Detailed studies of the excitation dynamics in photosynthetic pigment-proteins require an application of a wide range of spectroscopic methods. From the later part of the previous century, pump–probe and time-resolved fluorescence spectroscopy provided an impressive amount of information. Being simple to grasp, these methods are well-understood and widely used by the photosynthesis research community. In the last fifteen years, two-dimensional (2D) spectroscopy was developed. It has significant advantages over other methods, in particular higher temporal resolution available and higher signal-to-noise ratio. Even though it provides considerable opportunities in research, both its experimental realization and theoretical description are rather complicated, making it somewhat difficult to understand and apply. This makes an unfortunate gap in the community, with spectroscopy experts being able to use the technique, but sometimes lacking the relevant biological knowledge, while biologists having that knowledge are dubious about 2D spectroscopy due to the complexity of the approach. This publication is an attempt to fill this gap by providing an accessible introduction to the concepts, principles and possible applications of the 2D spectroscopy, aimed at the biologically trained members of the photosynthesis research community.

1. Introduction

Photosynthesis starts with the absorption of sunlight by specific pigments, namely (bacterio)chlorophylls, carotenoids and phycobilins, bound to the light-harvesting pigment-protein complexes [1]. The resulting excitation energy migrates between the light-harvesting complexes eventually reaching the reaction centers, where it triggers a fast charge separation. The quantum yield of this process is close to unity [2]. Following the discovery of the structure of the bacterial reaction center [3], high-resolution studies performed during the last decades revealed the structures of most of the pigment-protein complexes [2,4]. To understand the details of the mechanisms responsible for the high efficiency of the light reactions in relationship with the structural organization of the protein–pigment complexes, extensive efforts based on both theoretical and experimental approaches have been used.

Upon light absorption, separate molecules undergo a transition from the ground state to their excited states. In aggregated conditions the situation changes due to the resonance interaction between the electronic transitions of the pigment molecules. In this case, new collective energy levels are created with transitions to these levels being (partly) allowed and/or (partly) forbidden since excitations are intimately shared between molecules in the aggregate [5,6]. Absorption and fluorescence properties of such collective excitations known as Frenkel excitons depend on the relative orientations and positions of the interacting molecules. Spectral and dynamical properties of the photosynthetic molecular aggregates reflect a complex interplay of electronic excitations interacting with intra- and intermolecular vibrations. Indeed, the relative strengths of the intermolecular interaction and of the electron-vibration couplings are responsible for the ultrafast (femtosecond) dynamics that occurs in these complex systems [6].

Experimental characterization of the physical mechanisms underlying the fast processes in photosynthesis requires the development of time-resolved spectroscopic methods with the highest time resolution possible. Between the mid-'70s and the mid-'90s, following the development of the ultrashort pulsed light sources (mostly lasers) the nano- and picosecond time domains became accessible to pump–probe spectroscopy [7-12]. Nonetheless, the higher the time resolution wanted, the shorter must be the light pulses used in the experiments. Due to the Heisenberg uncertainty principle, the shorter the light pulse, the less defined is its energy. Therefore, when femtosecond time domain was reached, one was often forced to make trade-offs between spectral and temporal resolution.

To circumvent this unavoidable limit, an echo technique, now termed two-dimensional (2D) electronic spectroscopy, was formulated

* Corresponding author at: Institute of Chemical Physics, Faculty of Physics, Vilnius University, Sauletekio 9-III, 10222 Vilnius, Lithuania.
E-mail address: leonas.valkunas@ff.vu.lt (L. Valkunas).

https://doi.org/10.1016/j.bbabio.2018.12.006
Received 14 August 2018; Received in revised form 14 November 2018; Accepted 8 December 2018
Available online 21 December 2018
0005-2728/

at the turn of this century [13]. It provides information on the evolution of the system with both high time (reaching tens of femtoseconds) and spectral resolutions. This technique has now been widely employed on light-harvesting complexes and reaction centers [14-26] and led to a number of breakthroughs in the field.

Many excellent reviews on this spectroscopy already exist [13,27-34] along with books devoted partly or wholly to the subject [35-38]. Nonetheless, they are generally rather technical, delving deeply into either the experimental techniques or the theoretical concepts underlying the approach. Therefore, a review for a wide audience is still lacking. We are trying to fill this void. Here we aim to provide a comprehensive description of 2D spectroscopy for non-specialists. Our goal is to make this technique accessible to a broader audience, without complicating the subject. Therefore, we will try to simplify the subject as much as possible by focusing only on key points and avoiding exhaustive list of references.

This paper is organized as follows. First, in Section 2, we introduce the reader to experimental implementation of 2D spectroscopy by paying special attention to comparison with pump–probe spectroscopy. Then, in Section 3, we describe the concepts, conventions and information content of 2D spectroscopy. This is achieved by considering a series of model systems. Several examples on the wealth of information available from this technique are discussed in Section 4. Finally, in Section 5, we summarize our description and provide an outlook to further applications of 2D spectroscopy.

2. From pump–probe to 2D spectroscopy

For analysis of the dynamical properties of photosynthetic complexes the knowledge of the states involved, their energies and the excitation transfer rates between them is of the utmost importance. This knowledge can be obtained by using multidimensional spectroscopic techniques that allow one to excite specific states of the system and then monitor the response coming from the excited system states with the same or different energies. Multidimensional spectroscopies thus provide excitation frequency, detection frequency, and time-resolved spectroscopic data. It can be most naturally represented as time-resolved 2D maps, with one axis representing the excitation, and the other — the detection frequency. Each time point then corresponds to a different map. Various experimental approaches have their own advantages and disadvantages relating to resolution, noise, etc. In this section, we will provide a short overview of several of these techniques. In Fig. 1, we present schematic representations of these different experiments, together with a short description on how to obtain the time-resolved 2D maps and the advantages and disadvantages of each of these approaches. A similar description was given in a recent review of the experimental techniques of 2D spectroscopy [32].

In pump–probe spectroscopy, as demonstrated in Fig. 1a, a strong pump pulse (often narrow-band) with central frequency ω_{pump} excites the sample. After a delay time t_{delay}, a typically weaker probe pulse (usually spectrally wide) probes the sample, the resulting signal is recorded by a detector and the difference of the signals with pump and without pump pulse is obtained. A single experimental run thus gives a linear spectrum (depending on ω_{probe}) that represents a broadband detection after t_{delay} since the excitation of the sample with ω_{pump}. Repeating experiments with different ω_{pump} yields a 2D map corresponding to a specific t_{delay}. Observation of the temporal dynamics requires repetition of the procedure for different t_{delay}. Despite the apparent simplicity, this approach suffers from two major drawbacks. The first one is due to the interdependence of the time and excitation frequency resolutions. Narrow-band pulses, required for selective excitation, have wide envelopes in the time domain, thus obscuring the observed dynamics. Conversely, wide-band, short pulses cannot possibly be used for selective excitation. This technique is thus suitable when the events under observation are well-separated in time, or when the timescales of the processes are not too short. Additionally, pump–probe experiments are not background-free, since the relatively weak signal has to be separated from the probe pulse which simultaneously arrives at the detector. Therefore, the signal-to-noise ratio is limited, and the observation of weak features becomes difficult.

The latter limitation can be circumvented by the transient grating spectroscopy, illustrated in Fig. 1b. The single pump pulse is divided into two, with different spatial directions. After the interaction with the probe, the sample emits the signal in the phase matching direction that differs from the probe pulse, thus no background signal pollutes the detection. This phenomenon can be interpreted as if the pump pulses create a grating of matter response, thus leading the probe pulse to undergo a Bragg diffraction, resulting in an emitted signal at different direction. In this technique the 2D maps are obtained as in the pump–probe configuration. Correspondingly, the essential issue of interdependence of the excitation frequency and time resolutions remains.

Excitation frequency and time resolutions can be decoupled using the Fourier transform methodology [13]. The simplest experimental implementation of this approach is the colinear self-heterodyne 2D spectroscopy [39], illustrated in Fig. 1c. The pump pulse is split into two (using a pulse shaper, for example) with the same wavevector, giving access to an additional adjustable time delay. Following the accepted nomenclature, the delay between the pump pulses is often called the coherence time and denoted by t_1 (or τ), the delay between the second pump pulse and the probe pulse is called the waiting time and is denoted by t_2 (or T, it corresponds to t_{delay} in the pump–probe and transient grating experiments), and the delay between the probe pulse and the registered signal is called the detection time and is denoted by t_3 (or t). The signal as a function of detection frequency ω_3 is measured. In such experiment, the resolution in excitation frequency is not obtained by scanning the central frequency of the pump pulse, but by scanning the t_1 delay between the short broad-band pump pulses, and applying the Fourier transform over it. The excitation frequency is thus denoted as ω_1. In this approach, there is no interdependence of the excitation frequency and time resolution, as the employed pulses can be as short as necessary. Nevertheless, because the geometry is that of pump–probe spectroscopy, this technique also suffers from large background signal.

Combining both the transient grating and the colinear 2D spectroscopy leads one to the non-colinear heterodyne 2D spectroscopy, illustrated in Fig. 1d. In this case the pump pulses are separated both in spatial direction and in time, thus the excitation frequency and time resolutions are decoupled (because of Fourier transform methodology) and, additionally, the technique is background free (by detecting in direction different from the probe pulse). Moreover, detection is often made easier by the use of an additional local oscillator (LO) pulse. The 2D maps are obtained by scanning the delays t_1, t_2, measuring the signal depending on ω_3, and performing the Fourier transform over t_1. This technique is the current state of the art, and this is what we will have in mind when we refer to the *2D spectroscopy* later in the text.

In this section, we presented the different spectroscopic techniques schematically, highlighting only the most important differences. Detailed exposition on the different experimental implementations can be found in Refs. [13, 30-34].

3. Basic principles of 2D spectroscopy

In the previous section, we introduced the experimental basis of 2D spectroscopy. In this section, its basic concepts, notation and conventions will be explained using the schematic representations shown in Figs. 2– 12.

3.1. 2D spectra of model systems

3.1.1. Single two- or three-level systems

First, let us consider a two-level system (2LS) as the simplest model

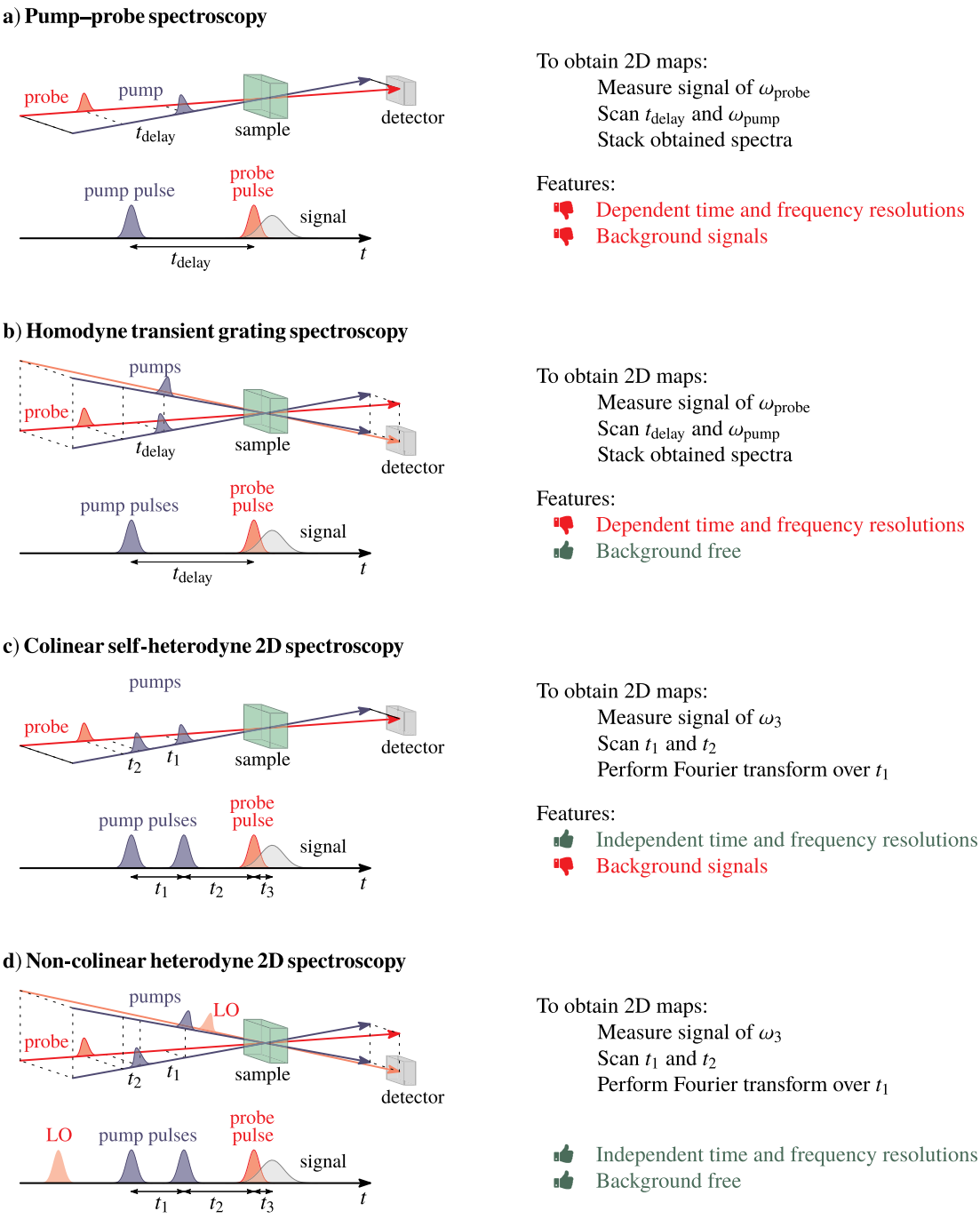

Fig. 1. Schemes of multidimensional spectroscopies that can provide time- and excitation/detection frequency-resolved information. **a)** Pump–probe spectroscopy. **b)** Homodyne transient grating spectroscopy. **c)** Colinear self-heterodyne 2D spectroscopy. **d)** Non-colinear heterodyne 2D spectroscopy. Top left (all parts), the spatial arrangement of the pulses, sample and detector; bottom left (all parts), temporal arrangement of the pulses and signal; right, the procedure to obtain 2D maps and characteristic features of the technique.

usually used to describe the optical transitions in a monomer. The 2LS is characterized by two energy levels, the ground state g and the excited state e. Therefore, the single parameter defining this system is the difference between the energies of these levels ω_{eg} (which coincides with the transition frequency), as shown on the left of Fig. 2a. Here and in the rest of the manuscript, we set $\hbar = 1$ and use frequency units for energy. The 2D spectrum of such system at zero waiting time ($t_2 = 0$) is displayed in the central part of Fig. 2a. The horizontal axis corresponds to the excitation frequency, ω_1, which increases from left to right, and the vertical axis corresponds to the detection frequency, ω_3, which increases from down to up. This is perhaps the most often used convention, but sometimes 2D spectra are plotted with excitation and detection axis interchanged (this is very common in 2D IR), or using wavelength instead of frequency. The 2D spectrum is typically expressed in electric field units, contrary to pump–probe spectra, that are expressed in optical density units. This means that the signs of the 2D and pump–probe spectra are opposite. Also note that there is no universal agreement on neither the number nor the exact positioning of the contour lines (in this paper we employ linear scale with solid lines for positive and dashed lines for negative amplitudes), nor the color scheme used to represent the 2D data (though the scheme employed here is encountered often in literature).

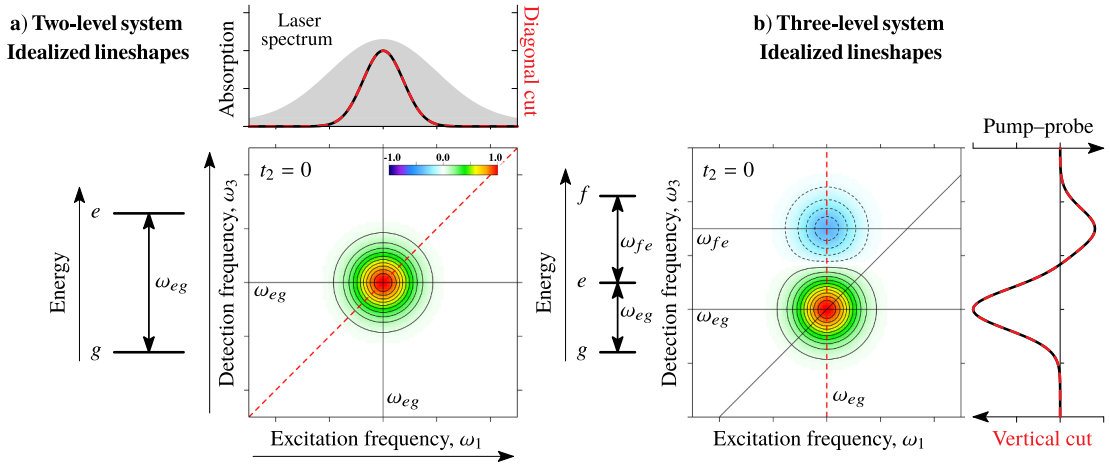

Fig. 2. Example 2D spectra of two- or three-level systems. **a)** Left, energy level diagram of a two-level system (2LS); top, absorption spectrum of the system (black solid line), along with the excitation laser spectrum assumed in experiments (grey shaded area) and diagonal cut of 2D spectrum (red dashed line); center, 2D spectrum of a 2LS with an idealized lineshape at zero waiting time. **b)** Left, energy level diagram of a three-level system (3LS); center, 2D spectrum of a 3LS with an idealized lineshapes at zero waiting time; right, vertical cut of 2D spectrum (red dashed line) and pump–probe spectrum of the system (solid black line). (For interpretation of the references to color in this figure legend, the reader is referred to the web version of this article.)

In the 2D spectrum given here, only one positive peak is visible, corresponding to the transition between the ground and excited states and determined by the ground state bleaching (GSB) and the excited state emission (ESE) contributions (their physical origin is the same as in pump–probe spectroscopy). It is centered at ω_{eg} in both excitation and detection axis. Note that the peak here is presented with an idealized lineshape, which is a two-dimensional Gaussian. For this system the 2D spectra remain constant throughout the waiting time t_2. On the top side of Fig. 2a the absorption spectrum of this system is displayed by the solid black line. The laser spectrum is assumed to entirely cover the absorption spectrum of the system (this is also the case in other figures, unless explicitly noted otherwise) and is given by the grey shaded area. For an ideal 2LS, the diagonal cut (with $\omega_1 = \omega_3$) of the 2D spectrum at zero waiting time can be scaled to match the absorption spectrum, as shown by the dashed red line.

A slightly more complicated example is a three-level system (3LS), which is illustrated in Fig. 2b. On the energy diagram (left), a higher excited state *f* is present in addition to the ground state *g* and the excited state *e*. The energy difference between states *f* and *e* is ω_{fe}, which is here assumed to be larger than ω_{eg}. The corresponding 2D spectrum at zero waiting time (central part of Fig. 2b) contains, besides the positive peak, a negative peak, centered at excitation frequency ω_{eg} and detection frequency ω_{fe}. This peak arises from the excited state absorption (ESA), thus possesses a negative amplitude. For this simple system the vertical cut of 2D spectrum (right, red dashed line) can be scaled to match the pump–probe spectrum plotted in electric field units (black line).

Usually, 2D spectroscopy is performed on an inhomogeneous ensemble of systems. Constituent molecules often have slightly different electronic excitation energies due to the slow degrees of freedom of their surroundings (solvent or protein). The system is then considered as having energetic disorder. This affects the 2D spectra of a simple 2LS as shown in Fig. 3. The energy level diagram illustrates a large number of non-interacting 2LSs with similar transition frequencies, composing the observed system. The 2D spectra of such an ensemble is displayed in the right panel, with the corresponding absorption spectra shown above. The peak shape in the 2D spectrum becomes a non-symmetric Gaussian, and its width along the diagonal and antidiagonal corresponds to inhomogeneous and homogeneous broadening, respectively (compare to the absorption spectrum of the ensemble, given by the thick black line, and the single constituent absorption, given by thinner blue lines). Strictly speaking, the antidiagonal width corresponds to a

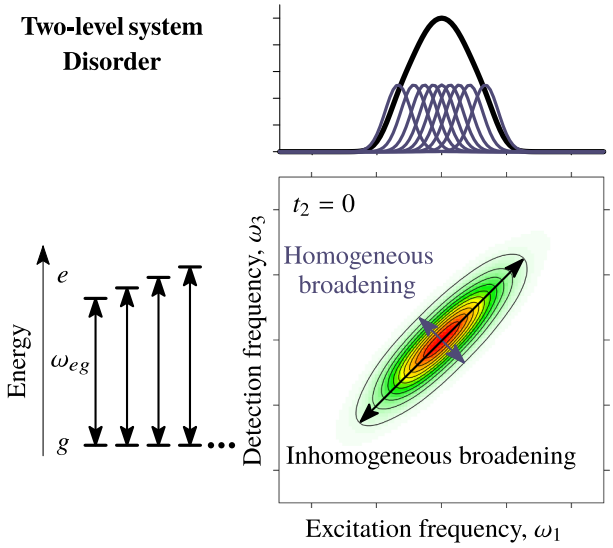

Fig. 3. Example 2D spectra of a 2LS with disorder. Left, energy level diagram of a 2LS with disorder (inhomogeneous ensemble of two level systems); right, 2D spectrum of an ensemble of 2LSs at zero waiting time; top, absorption spectra of the corresponding ensemble (thick black line) and its constituents (thinner blue lines). (For interpretation of the references to color in this figure legend, the reader is referred to the web version of this article.)

convolution of a homogeneous lineshape and the inhomogeneous distribution of the transition frequencies, and can be denoted as total broadening, but we will not make such distinction here. The possibility to directly separate the homogeneous and inhomogeneous broadening is an advantage of 2D spectroscopy.

In real experiments, the lineshapes of the peaks in the 2D spectra are rarely simple two dimensional Gaussians as they are determined by the interactions between the electronic and vibrational degrees of freedom. Examples of 2D spectra with realistic lineshapes are given in Fig. 4. First, in Fig. 4a realistic lineshapes of a single two level system are shown. On the left, in the energy level diagram, the curved lines illustrate the potential energy surfaces of the ground state *g* and the excited state *e* along some generalized coordinate. The energy surface of the excited state is shifted relative to the ground state. Therefore, transitions do not occur between the minima of the surfaces, and subsequent relaxation takes place (on the order of time τ_{rel}). Accordingly,

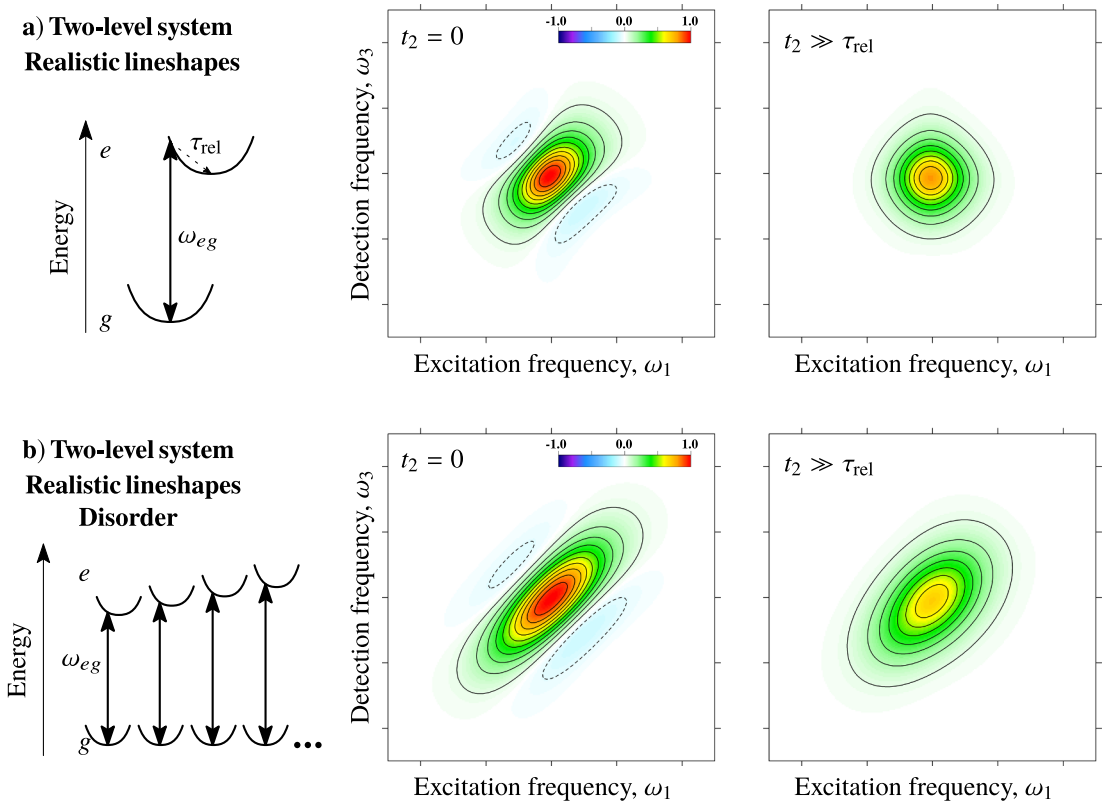

Fig. 4. Example 2D spectra of a 2LS (without or with disorder) with realistic lineshapes. **a)** Left, energy level diagram of a realistic 2LS, illustrating potential energy surfaces along some generalized coordinate; right, 2D spectra of a 2LS with realistic lineshapes at zero and long waiting times. **b)** Left, energy level diagram of a realistic 2LS with disorder; right, 2D spectra of a realistic two level system with disorder at zero and long waiting times. Calculations of these 2D spectra were performed using the approach described in Ref. [35].

the 2D spectra will evolve during the waiting time t_2, as shown in the right panel of Fig. 4a. While at zero waiting time the 2D peak is not symmetric, elongated along the diagonal, and accompanied by negative lobes on its sides, after a waiting time longer than relaxation ($t_2 \gg \tau_{rel}$), its shape becomes almost round. This is related to the loss of the memory of excitation — no matter at what frequency the system was excited, it emits from the thermally equilibrated excited state (corresponding to a thermal distribution).

When disorder is added to such a realistic 2LS, at zero time the peak in the 2D spectrum is more elongated diagonally than in Fig. 4a, and similarly as in Fig. 2c (see Fig. 4b, right panel). With time, the anti-diagonal width of the peak increases, but the peak does not become round. Thus, contrasting the 2D spectra at $t_2 \gg \tau_{rel}$ in both Fig. 4a and b, we see that a homogeneous system exhibits round peaks in the 2D spectra at longer times, while the peaks of an inhomogeneous system remain elongated along the diagonal. This qualitative difference is useful in the analysis of experimental data. A nice example of evolution of a spectral lineshape of a 2LS is given in Ref. [40], where chlorophyll *a* was studied.

3.1.2. Two coupled two-level systems — a dimer

Let us now consider a more complicated situation, i. e. a dimer consisting of two resonantly coupled 2LSs. The 2D spectrum of a dimer, along with the illustrating diagrams, is shown in Fig. 5. The transition dipole moments (left of the figure) are assumed to be at some angle, and, due to the close vicinity of the monomers, resonance interaction between the molecular excited states is not negligible. In the energy diagram (central part of the figure), both molecules have their own ground states, their excited states are denoted by *a* and *b*, and the transition frequency of monomer *a*, ω_{ag}, is assumed to be smaller than that of monomer *b*, ω_{bg}. Due to the resonance interaction, the molecular states are no longer the eigenstates of the dimer, which are the delocalized excitations, termed excitonic states or excitons [6]. The energy gap between the excitonic states e_1 and e_2 is larger than the energy gap between the molecular states *a* and *b*, because of the energy level repulsion. A double-excited state *f* also appears, which corresponds to the situation when both excitonic states are excited at the same time. Transitions $e_2 \leftrightarrow g$ and $f \leftrightarrow e_1$ are somewhat stronger in this example, thus are drawn with thicker lines.

The 2D spectrum of such a system (Fig. 5, right panel) at zero waiting time contains four peaks at excitation and detection frequencies matching the transition frequencies of the excitonic states ω_{e_1g} and ω_{e_2g}. In addition to the diagonal peaks, crosspeaks can also be observed, arising from the coupling between the monomers. Since they would not be present if the interaction between the molecular states was negligible, their presence at very early time in 2D spectra implies coupling between the constituents of the observed system. The lower crosspeak is negative, which indicates that the ESA signal is stronger than the corresponding ESE and GSB signals. Note, that this depends on the spatial arrangement of the constituent transition dipole moments. Above this 2D spectrum the corresponding absorption spectrum (solid black line) and the diagonal cut of the 2D spectrum (dashed red line) are plotted. For a systems containing more than a single 2LS, the diagonal cut can no longer be scaled to match the absorption spectrum, as the peak amplitude is proportional to the square of the transition dipole moment in the absorption spectrum, and to the fourth power of the transition dipole moment in the 2D spectrum.

The time-evolution of this 2D spectrum is shown in Fig. 6. In the diagram of the energy levels (left panel), the transition rates between the excitonic states ($k_{e_1e_2}$ and $k_{e_2e_1}$) are introduced. Their sum defines the excitation equilibration timescale in the system. 2D spectra at times $t_2 = 0$ and at time when the energy transfer is completed, i. e.

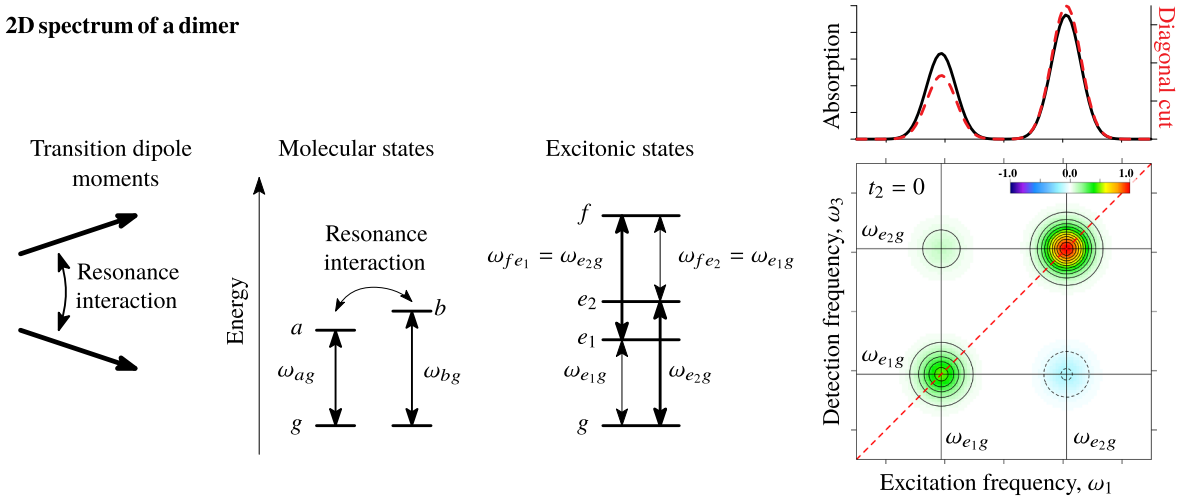

Fig. 5. Example 2D spectrum of a dimer — two coupled 2LSs. Left, depiction of the orientation of the transition dipole moments; center, energy level diagrams depicting both the molecular and the excitonic states; right, 2D spectrum of such a system at zero waiting time; top, corresponding absorption spectrum (solid black line) and the diagonal cut of the 2D spectrum (red dashed line). (For interpretation of the references to color in this figure legend, the reader is referred to the web version of this article.)

$t_2 \gg 1/(k_{e_2e_1} + k_{e_1e_2})$, are plotted in the top and bottom rows of the figure, respectively. At long waiting time, the diagonal peak at $\omega_1 = \omega_3 = \omega_{e_2g}$ shows a considerable loss of amplitude, because the excitation energy was transferred from e_2 to e_1. The lower crosspeak, correspondingly, shows a large increase of the signal amplitude, even going from negative to positive. On the other hand, dynamics of peaks at excitation frequency ω_{e_1g} is much less pronounced. Nonetheless, the diagonal peak shows some loss of the amplitude, because of the uphill excitation transfer from the lower excitonic state to the higher one. This is possible at higher temperatures, when the thermal energy k_BT is of similar magnitude to the energy gap between the excitonic states. Correspondingly, the crosspeak shows some increase of the amplitude. Vertical cuts of the 2D spectrum at excitation frequency ω_1 equal to ω_{e_1g} or ω_{e_2g} (denoted in the figures by red and blue lines respectively), in principle, can be compared to narrow-band pump-probe experiments (relation of 2D spectra and pump-probe spectra will be discussed in more detail later, see Section 3.2). Red line shows larger intensity at the detection frequency $\omega_3 = \omega_{e_1g}$, while the amplitude of the crosspeak is

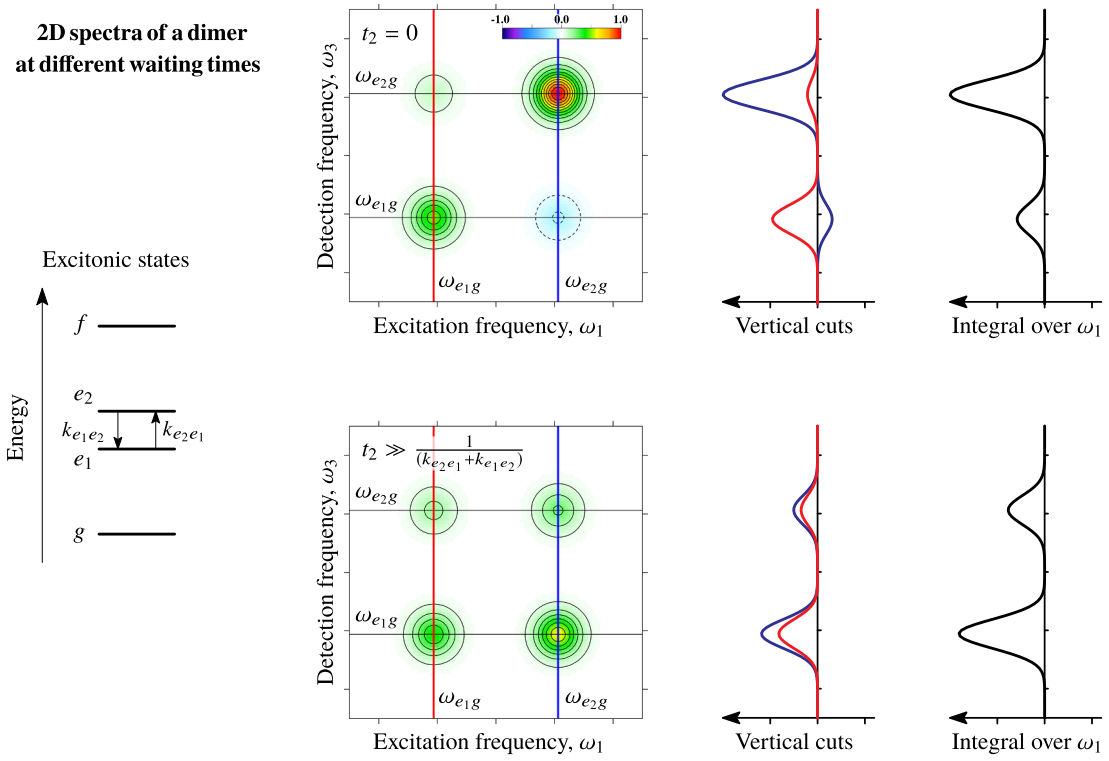

Fig. 6. Example 2D spectra of a dimer at different waiting times t_2. Left, the energy level diagram of the excitonic states of the system, with transition rates ($k_{e_1e_2}$ and $k_{e_2e_1}$) defined between the excitonic states e_1 and e_2; top row, 2D spectrum of a dimer at waiting time t_2 equal to zero, vertical cuts (red and blue curves) of the 2D spectrum at excitation frequencies equal to ω_{e_1g} and ω_{e_2g}, and integral over excitation frequency ω_1; bottom row, same as top row, but at waiting time $t_2 \gg 1/(k_{e_2e_1} + k_{e_1e_2})$, that is, after relaxation between the excitonic states is complete. (For interpretation of the references to color in this figure legend, the reader is referred to the web version of this article.)

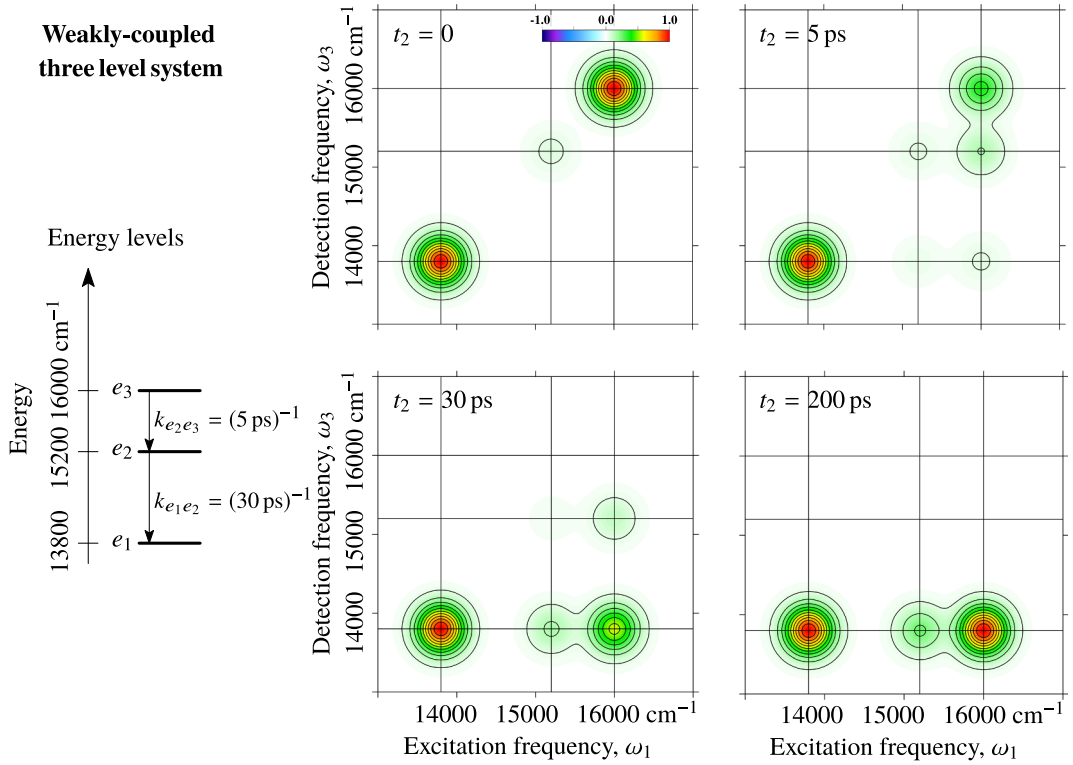

Fig. 7. 2D spectra of a weakly coupled three-level system. Left, the energy level diagram of the system, with downwards transition rates ($k_{e_1e_2}$ and $k_{e_2e_3}$) defined; right, 2D spectra at representative waiting times t_2. The transitions to state e_2 are taken to be twice as weak as those to e_1 and e_3.

much smaller at the initial time. The blue line shows larger intensity at $\omega_3 = \omega_{e_2g}$, while the amplitude of the crosspeak is negative. At longer times the amplitudes of the cuts become somewhat similar, with features corresponding to lower detection frequency having larger amplitudes. The integral of the 2D spectrum over the excitation frequency ω_1, can be compared to a wide-band pump-probe spectrum. It shows a more global picture — decrease of the amplitude at higher energy and increase of the amplitude at lower energy with increasing waiting time.

3.1.3. Weakly coupled three-level system

In this subsection, we will consider a weakly coupled 3LS, to demonstrate how energy transfer in such case is represented in the 2D spectra. This situation corresponds to the well-known Förster regime of energy transfer. In the left of Fig. 7, we show the energy levels of our example system. Please note that here this 3LS describes three weakly-coupled molecules rather than a single molecule with three energy levels as in Fig. 2b. The states here are assumed to be only weakly coupled, so that energy relaxation is possible. We also assume that only downwards energy transfer rates are present, with the timescales differing substantially. Energetically upwards transfer rates would be negligible for gaps much larger than the thermal energy. The rate between closer lying energy levels is taken to be 6 times faster than that between the further energy levels. This represents a possible realistic scenario.

Let us now turn our attention to the 2D spectra given on the right of Fig. 7. At initial waiting time $t_2 = 0$, we see only the diagonal peaks, indicating that coupling between the energy levels is negligible. This is in stark contrast with previously discussed example of excitonic dimer, where 2D spectra showed crosspeaks at the earliest times. Note also that the diagonal peak corresponding to transitions to e_2 level is considerably weaker than the others. We have taken this transition to be weaker with a factor of two and this translates to the peak being 16 times weaker. This is because the peak amplitudes in the 2D spectra scale as the fourth power of the corresponding transition dipole moments.

With increasing waiting time, the 2D spectra show loss of amplitude in the diagonal peaks and corresponding increase of amplitudes of lower crosspeaks. These spectral dynamics provide information about the energy transfer pathways in the system. Consider the two crosspeaks at excitation frequency $\omega_1 = 16{,}000\,\mathrm{cm}^{-1}$. At waiting time $t_2 = 5$ ps, the one at detection frequency $\omega_3 = 15{,}200\,\mathrm{cm}^{-1}$ has larger amplitude than that at $\omega_3 = 13{,}800\,\mathrm{cm}^{-1}$, and the situation is reversed at waiting time $t_2 = 30$ ps. This suggests that the e_2 state is an intermediate state in energy relaxation cascade from e_3 to e_1, as is indeed the case for our chosen system. Similar considerations can help to extract information about the cascades of energy transfer from actual experimental 2D spectra as well.

Another important point related to the 2D spectra of a weakly-coupled system is that at long waiting times the diagonal peaks corresponding to higher energy levels vanish, and only crosspeaks related to the lowest state remain, as can be seen in the 2D spectra corresponding to $t_2 = 200$ ps in Fig. 7. Of course, this might not be entirely the case if energy levels are closer in energy and some upwards energy transfer is possible.

To summarize, the key differences between the 2D spectra of weakly- and strongly-coupled systems are that no crosspeaks are visible at initial waiting times and no diagonal peaks corresponding to the higher energy levels are visible at long waiting times in the former case.

3.2. Comparison of 2D and pump–probe spectroscopies

The decoupling of time and frequency resolutions is one of the main advantages of 2D spectroscopy versus pump–probe spectroscopy. In this subsection, we will provide a simplified explanation for these differences. To keep the discussion simple, we will neglect the influence of the pulse overlap effects.

The resolution can be defined along three axis: excitation frequency (ω_1 or ω_{pump}), detection frequency (ω_3 or ω_{probe}) and waiting time (t_2 or

t_{delay}). The influence of the laser pulses to the 2D or pump–probe spectra can be expressed as:

$$2D(\omega_1, t_2, \omega_3) = 2D_{ideal}(\omega_1, t_2, \omega_3) \times \text{Wide band pulse}(\omega_1) * \text{Short pulse}(t_2) \times \text{Wide band pulse}(\omega_3); \quad (1)$$

$$PP(\omega_1, t_2, \omega_3) = 2D_{ideal}(\omega_1, t_2, \omega_3) * \text{Pump pulse}(\omega_1) * \text{Pump pulse}(t_2) \times \text{Wide band (probe) pulse}(\omega_3). \quad (2)$$

Here, $2D_{ideal}(\omega_1, t_2, \omega_3)$ is the ideal 2D spectrum of the system, determined only by the system's characteristics, and the symbols × and * mean multiplication and convolution, respectively. In both the 2D and pump–probe spectroscopy experiments, the detection frequency resolution is obtained by multiplying the system response with the laser pulse in the frequency domain. Since it is common that the laser pulse is spectrally wide, thus covering every relevant transition band, the detection frequency resolution can be very close to the ideal case. Of course, if the laser pulse is narrower than the spectral bandwidth of the system, some of the spectroscopic features near or outside the spectral window become unresolvable (see also discussion in Section 3.3). The main differences between the 2D and pump–probe spectroscopies lie in the waiting time and excitation frequency resolution. In 2D spectroscopy, the excitation frequency resolution is determined in the same way as the detection frequency resolution — the system response is multiplied by the laser pulse in the frequency domain. The time resolution, meanwhile, is obtained by convolving the system response with the laser pulse in the time domain. Since the laser pulse is broad in the frequency domain, and thus short in the time domain, both excellent time and excitation frequency resolutions can be achieved. This is in a strong contrast with pump–probe spectroscopy. There the convolution in the time domain is also employed to obtain the waiting time resolution. Yet to obtain the excitation frequency resolution, the convolution in the frequency domain must be employed with the *same* (pump) laser pulse. The key issue is that short pulses in the time domain mean wide pulses in the frequency domain and, conversely, long pulses in the time domain mean narrow pulses in the frequency domain. Thus, in the narrow band pump–probe (long pump pulse) conditions, selective spectral excitation is achieved, but at the cost of the time resolution, and wide band pump–probe (short pump pulse) experiments have good time resolution, but are not able to discern spectral features. 2D spectroscopy, however, combines the advantages of both approaches.

To further illustrate this description, in Fig. 8, we show a comparison of frequency and time resolutions in an ideal 2D experiment, a realistic 2D experiment, and a realistic pump–probe experiment. The system under consideration is a dimer, with two excitonic states separated by 150 cm^{-1} (Fig. 8b), a downhill energy transfer rate of $(100\ fs)^{-1}$ and an uphill rate calculated from the detailed balance relation (assuming the experiment is performed at 300 K) of $(205\ fs)^{-1}$. These numbers represent typical values of photosynthetic complexes [6].

In the ideal 2D experiment, the width of the laser pulse in the time domain tends to zero (full width at half maximum $FWHM_t \to 0$), while the width in the frequency domain is infinite ($FWHM_\omega \to \infty$). For the realistic 2D experiment, the width of the laser pulses was fixed at $FWHM_t \approx 12$ fs (or standard deviation $\sigma_t = 5$ fs), which is close to state-of-the-art with current experimental setups [41-43]. Accordingly, in the frequency domain the laser pulses have a width of $FWHM_\omega \approx 2500\ cm^{-1}$ (or $\sigma_\omega \approx 1060\ cm^{-1}$). Finally, for the realistic pump–probe experiment, the pump pulse, which controls the excitation frequency and time resolution, was chosen with $\sigma_t = 50$ fs (or $FWHM_t \approx 120$ fs) in the time domain, and $FWHM_\omega \approx 250\ cm^{-1}$ (or $\sigma_\omega \approx 106\ cm^{-1}$) in the frequency domain. In the frequency domain the center frequency of the pulses was set at 15,000 cm^{-1}, in the middle between the energies of the two exciton states.

Fig. 8a shows the comparison of the 2D maps at two different waiting times. The ideal 2D spectra show four clearly resolvable peaks (two diagonal peaks and two crosspeaks) centered at the transition frequencies ω_{e1g} and ω_{e2g}. The realistic 2D spectra are very similar at both delay times demonstrating the excellent resolution that can be achieved in the 2D experiments. The 2D maps showing the pump–probe data sets can be obtained by stacking many pump–probe experimental data sets obtained at different excitation (pump) frequencies. Assuming the experiments are performed in more or less identical conditions, the stacked pump–probe 2D maps then show the same kind of information as the maps of 2D spectroscopy, albeit with less details. In recent years, this type of pump–probe data stacking is employed usually in the UV region [44,45], though applications for visible range also exist [46]. In the simulated case presented here, the 2D maps showing the realistic pump–probe spectra are substantially different than the ones of 2D spectroscopy. First, due to the loss of the excitation frequency resolution, it is not possible to discern four separate peaks – only two peaks, at detection frequency equal to ω_{e1g} or ω_{e2g} are visible. Moreover, while the lower crosspeak should be negative, there is no negative amplitude in pump–probe spectra. This can, for instance, prevent extraction of information about the relative orientation of the transition dipole moments. At longer delay times, the maximum of the peak corresponding to detection frequency equal to ω_{e1g} shifts along the excitation frequency axis, suggesting that there should be at least two states, which are clearly resolved in 2D spectra. Interpretation of the pump–probe data thus often requires more *a priori* knowledge about the system.

Finally, Fig. 8c depicts the dynamics of a diagonal peak D1 and crosspeak CP1. While the curves corresponding to realistic 2D and ideal 2D are very similar, pump–probe data show considerable differences. For the diagonal peak D1, the slow rise of the amplitude results from a convolution with the laser pulse in the time domain, causing difficulties to determine the real decay time. In addition, the relative long time amplitude of the D1 peak is much larger than in the 2D case. For the crosspeak CP1, the dynamics clearly shows an offset amplitude, as discussed before, and the rise time looks slower due to the convolution effects.

It must be noted, however, that the resolution deficiencies of pump–probe spectroscopy become important only when the system under consideration has several close bands with fast dynamics. If the spectroscopic bands are well separated and the timescales of interest are longer, pump–probe spectroscopy is able to provide the same answers as 2D spectroscopy. Nonetheless, one significant advantage of the latter is that a system with many energy levels can be investigated by a single experiment, instead of several narrow-band pump–probe experiments, each of them selectively exciting a different state.

3.3. Two-color 2D spectroscopy

Often, the laser pulses in 2D experiments can completely cover all the bands of interest. This is illustrated in Fig. 9a. In such a case, the obtained 2D spectrum shows all relevant features, making examination of data relatively easy. Nevertheless, situations may occur when the bands of interest are spectrally well-separated. A possible example of this situation is when one wants to observe dynamics in both S_2 bands in carotenoids and in Q_y bands in chlorophylls at the same time [47]. Then it is hardly possible to see all the diagonal peaks and the crosspeaks in a 2D spectrum from a single experiment. By repeating experiments with shifted central frequency of the laser pulse, information can be obtained about all the diagonal peaks. Unfortunately, single-color 2D spectroscopy sometimes cannot provide information about the crosspeaks that are located too far from the diagonal, as is shown in Fig. 9b. In contrast to a popular belief that 2D spectroscopy experiments can only address these relatively narrow spectral windows, while pump–probe spectroscopy has no such shortcoming, the full set of information from such a system can nonetheless be obtained by using the two-color 2D spectroscopy.

Conceptually, it is similar to the two-color pump–probe spectroscopy — excitation at one frequency (or color) and detection at another. Nonetheless, due to the experimental difficulties, the two-color 2D

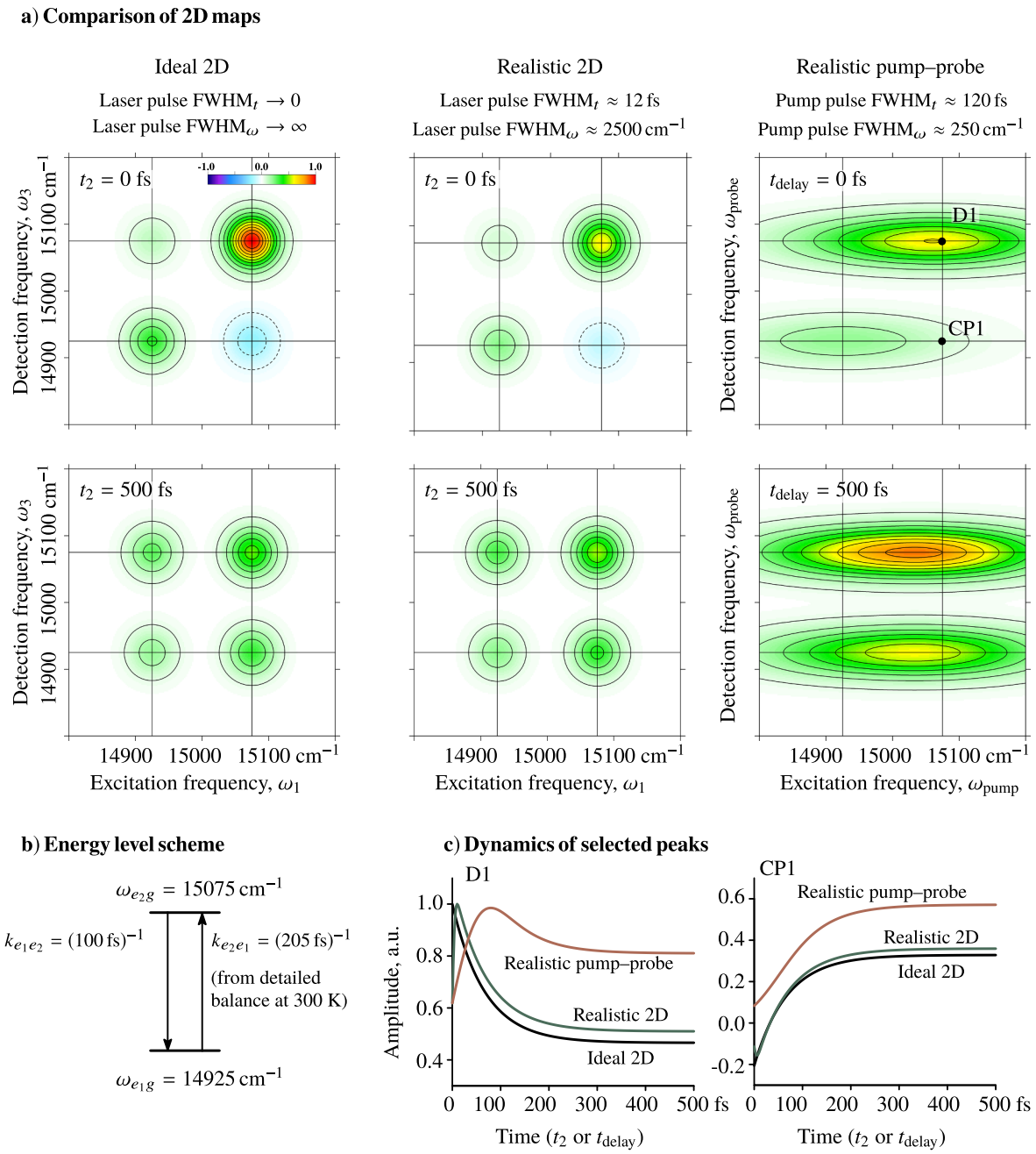

Fig. 8. Comparison of the frequency and time resolution provided by an ideal 2D spectroscopy experiment, a realistic 2D spectroscopy experiment and a realistic pump–probe spectroscopy experiment of a model dimer system. **a)** Comparison of 2D maps at two waiting times. **b)** Energy level scheme of the system, depicting the energy transfer rates. **c)** Dynamics of the diagonal peak D1 and crosspeak CP1.

spectroscopy is relatively rarely employed. In Fig. 9c and d, we illustrate the fundamental concepts of this approach. Extracting the crosspeaks requires the tuning of the pump and probe pulses to different colors. Thus, by pumping and probing at different frequencies, distinct areas of a full 2D map can be obtained. In Fig. 9c, it is shown that by pumping at the red part of the absorption spectrum and probing at the blue part one can obtain the upper crosspeak region. On the other hand, pumping at the blue and probing at the red allows to obtain the lower crosspeak, see Fig. 9d. Of course, the two-color 2D spectra may contain more than a single crosspeak. Then centering the laser pulses to cover as many bands as possible becomes not trivial. Nonetheless, by careful application of the two-color 2D spectroscopy one can reconstruct the entire 2D map that would be available from an ideal 2D experiments with sufficiently broad pulses.

Here, an additional point about the effect of laser pulses can be noted — they can distort the peak shape if they do not cover it entirely. This can be most clearly visualized by comparing Fig. 9a and c. When the laser pulses are spectrally wide, the maxima of the upper crosspeaks perfectly match the maxima in the absorption spectrum (Fig. 9a). On the other hand, in Fig. 9c, we can see that when the laser pulse is in between the actual peaks, their maxima become shifted in the 2D spectra. One must therefore be careful if perfect coverage of the absorption bands of interest cannot be achieved.

Note that another introductory presentation of the two-color 2D spectroscopy was made in Ref. [47], where this type of experiment was performed on the fucoxanthin-chlorophyll binding protein complex. This technique was also applied to study bacteriochlorophyll dynamics after carotenoid excitation in LH1 light-harvesting complex from

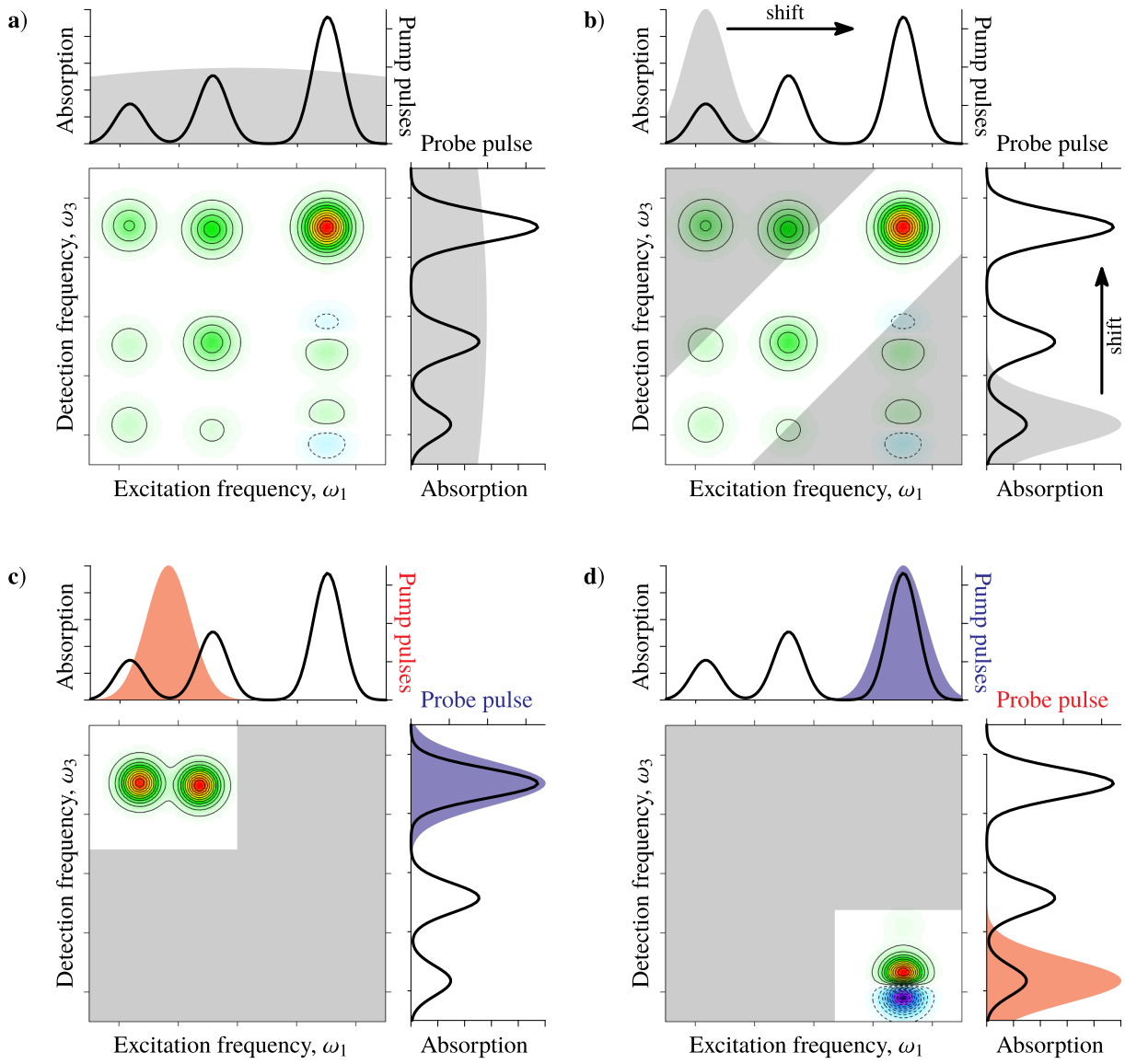

Fig. 9. Illustration of two-color 2D spectroscopy of a dimer. **a)** Center, broadband 2D spectrum of a complicated system; top, absorption spectrum (solid black line) and pump pulses (grey shaded area); right, absorption spectrum (solid black line) and probe pulse (grey shaded area). **b)** Center, bright areas – information available from single color 2D experiments using narrow pulses, grey areas – information unavailable from single color 2D experiments using narrow pulses; top, absorption spectrum (solid black line) and pump pulses (grey shaded area), the arrow indicates shifting of the central frequency of the pump pulses; right, absorption spectrum (solid black line) and probe pulse (grey shaded area), the arrow indicates shifting of the central frequency of the probe pulse. **c)** Center, red-blue 2D spectrum of a complicated system; top, absorption spectrum (solid black line) and pump pulses (red shaded area); right, absorption spectrum (solid black line) and probe pulse (blue shaded area). **d)** Center, blue-red 2D spectrum of a complicated system; top, absorption spectrum (solid black line) and pump pulses (blue shaded area); right, absorption spectrum (solid black line) and probe pulse (red shaded area). (For interpretation of the references to color in this figure legend, the reader is referred to the web version of this article.)

bacteria [48] and to investigate the $Q_y - Q_x$ crosspeaks in the bacterial reaction center [49]. Theoretically, two-color 2D spectroscopy was examined in detail for a molecular dimer in Ref. [50].

3.4. Analysis of 2D spectra

In this section, we will discuss different ways to present and analyze the data available from 2D spectroscopy. This is mostly illustrated in Fig. 10. The overall dataset comprises a cube of 2D spectroscopy data (see Fig. 10a), with one dimension being the excitation frequency ω_1, another – the detection frequency ω_3, and the third – the waiting time t_2. The 2D data is most often analyzed by taking cuts of this cube along some chosen dimensions.

Let us examine the 2D spectra at several waiting times of the model system depicted in Fig. 10b. It contains two excited states, e_1 and e_2, with possible transfer between them, and the higher energy state, e_2, also decays to the ground state (Fig. 10c). This corresponds to cuts of the full cube of 2D data at specific t_2 values. The first step of analysis should concern the 2D map corresponding to the earliest waiting time. It reveals the peak pattern, their position, the sign of the crosspeaks (and the homogenous and inhomogenous broadenings, though in the example here we choose ideal lineshapes for simplicity). Then, comparing the 2D maps at different waiting times, we can immediately notice a decrease of the amplitude of the diagonal peaks, and an increase followed by a later decrease of the amplitude of the crosspeaks. The lower crosspeak even changes the sign from negative at initial time to positive at later times.

Choosing the most interesting spectral features, we can analyze

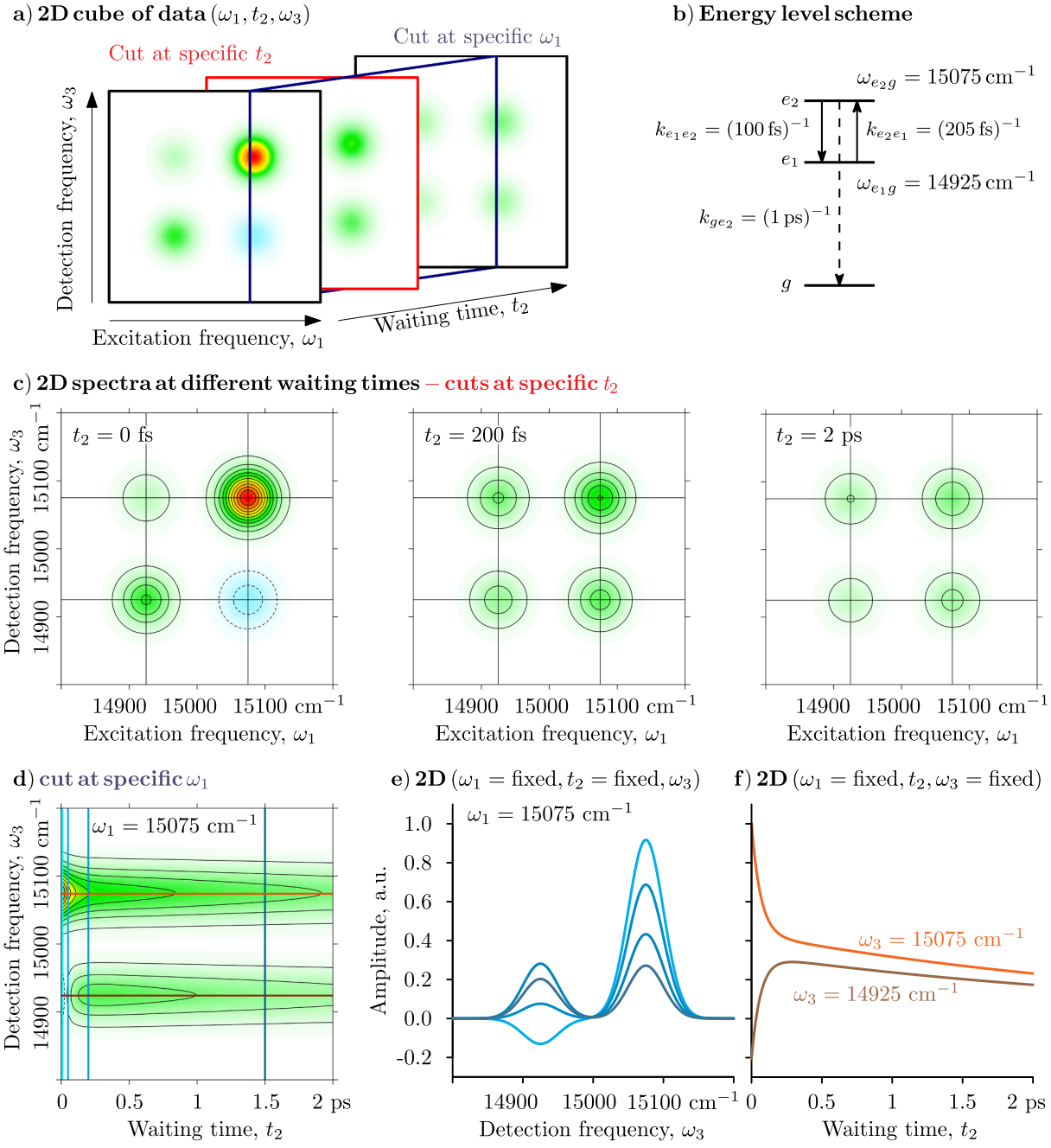

Fig. 10. Different ways of analyzing the 2D spectroscopy data. **a)** A graphical representation of the combined three dimensional (two frequency dimensions and one time dimension) data available from the 2D experiment, with colors highlighting specific cuts. **b)** Energy level scheme of the system, depicting the energy transfer rates. Not that the higher energy excited state can decay to the ground state. **c)** 2D spectra at different waiting times, corresponding to cuts of the full data cube at specific t_2. **d)** Cut of 2D data cube at specific excitation frequency $\omega_1 = 14{,}975\,\mathrm{cm}^{-1}$, with horizontal and vertical axis representing waiting time (t_2) and detection frequency respectively (ω_1). **e)** Cuts of the full cube of 2D data at specific excitation frequency $\omega_1 = 14{,}975\,\mathrm{cm}^{-1}$ at several waiting time (t_2) values. **f)** Cuts of full cube of 2D data at specific excitation frequency and detection frequency, representing kinetics of chosen spectral features. (For interpretation of the references to color in this figure legend, the reader is referred to the web version of this article.)

their temporal dynamics more closely. First, in Fig. 10d, we present a 2D plot corresponding to the cut of the full cube of 2D data along the specific value of the excitation frequency $\omega_1 = 15{,}075\,\mathrm{cm}^{-1}$. Thus, the horizontal axis here represents the waiting time t_2 instead of the excitation frequency. In this way, we see all the time evolution of the upper diagonal peak and the lower crosspeak. While this type of representation gives nice visualization, for more quantitative analysis it is more convenient to compare the cuts at different t_2 values, as is done in Fig. 10e. Here the colors of the lines correspond to colors of vertical lines in Fig. 10d. Thus, Fig. 10e depicts the cuts of the full data cube both at fixed excitation frequency ω_1 and fixed waiting time t_2. This type of plot allows to quantitatively compare the amplitudes of the spectral features at specific times. Another way to obtain the temporal dynamics of the selected spectral features is to simply plot their kinetics. This is done in Fig. 10f for the upper diagonal peak (orange line) and the lower crosspeak (brown line), with colors matching the horizontal lines in Fig. 10d. This representation corresponds to cuts of the full data cube at fixed excitation and detection frequencies. In this case, we can notice that there are two distinct timescales in the system. Fast timescale corresponds to decay of amplitude of the diagonal peak with

the corresponding increase of amplitude of the crosspeak, suggesting energy transfer. A slower timescale corresponds to the decay of both peaks, suggesting the relaxation of excitation to the ground state.

This discussion would not be complete without mentioning the analysis of 2D data in terms of the decay associated spectra (DAS). Though performed on pump–probe or time-resolved fluorescence datasets for decades, only recently this approach was applied to the 2D spectroscopy results with different implementations [17,47,51,52]. The main idea is to decompose the full 2D dataset into several distinct 2D spectra, each evolving with distinct timescale. The obtained spectra then correspond to some compartment in a chosen kinetic model (parallel, sequential, or more complicated). Mathematically, we write that the 2D spectra is described as a sum of products of spectral components and their time-dependent kinetics:

$$2\mathrm{D}(\omega_1, t_2, \omega_3) = \sum_{k=1}^{N} A_k(\omega_1, \omega_3) D_k(t_2). \tag{3}$$

Here, N is the number of independent components, $A_k(\omega_1, \omega_3)$ is the spectra of the k-th component and $D_k(t_2)$ is the kinetics of the k-th component. These populations have to be calculated based on the assumed kinetic model and then convoluted with a suitable instrument response function (IRF). Assuming a parallel model and a Dirac delta function for the IRF, the kinetics are simply $D_k(t_2) = \exp(-t_2/\tau_k)$, with τ_k being the decay timescale of the k-th component. The fitting procedure can be simplifed by using the pseudoinverse matrices to calculate the amplitude maps from the timescales, as described in Ref. [53]. More involved kinetics schemes are described in Ref. [54].

From the dataset of Fig. 10 one can obtain the DAS shown in Fig. 11. Here, we have chosen a simple parallel two compartment scheme, demonstrated in Fig. 11a. The obtained DAS with their timescales are given in Fig. 11b. In this case, the two DAS can be easily interpreted with the one with the fast timescale corresponding to the energy transfer between the excited states while the other corresponding to the overall relaxation to the ground state. Nonetheless, extreme caution must be applied when interpreting DAS for larger systems (larger photosynthetic complexes, their aggregates or even whole photosystems), as then the obtained DAS might not correspond to any physical processes, being instead a mathematical representation of complex non-exponential dynamics arising from multiple constituents, with possibly fluctuating spatial positions.

It must be noted that data analysis techniques are rapidly developing in this field. In Ref. [55], a novel way of using complex exponentials to describe both population dynamics and oscillatory features was reported. Another interesting approach to decompose the 2D data and obtain the species associated spectra was presented in Ref. [56].

3.5. Oscillatory dynamics in 2D spectra

Up to now, we completely ignored the possible oscillatory dynamics in the 2D spectra, even though they have been observed in experiments. This is because more often than not they just complicate the extraction of information about the relevant energy transfer processes in the system. Nonetheless, here we briefly describe how the oscillations manifest in the 2D spectra. Consider a similar excitonic dimer as was presented in Fig. 8b, but with the gap between excitonic states being 300 cm^{-1} and the downhill energy relaxation rate being $(400\ \mathrm{fs})^{-1}$. For the present demonstration, we will also assume that coherent contributions to the 2D spectra are present, and their decay timescale is taken to be 200 fs. In Fig. 12a, we plot a zero waiting time 2D spectrum of this system and we also mark the two diagonal peaks and two crosspeaks. Their respective dynamics including the oscillatory contributions are shown in Fig. 12b. We clearly see that in this case the coherent contributions manifest as small amplitude oscillations, which are additive to the signals that follow population dynamics. The period of oscillations in this case is related to the energy gap between the two excitonic states, with $\omega_{e_2e_1} = 300\ \mathrm{cm}^{-1}$ giving the period of ≈ 110 fs. In this case, the influence of coherent oscillatory contributions is relatively minor, and relevant population kinetics can be inferred from the peak dynamics. On the other hand, oscillations might hinder the extraction of the relevant energy transfer timescales when their amplitude becomes larger.

Here, our simulations reflected possible electronic coherence contributions. Their origin is due to the phase relationship between the excitonic states. They manifest as oscillations in both diagonal peak and crosspeak dynamics and their influence is stronger when the constituents of the system are coupled more strongly. In case of weakly-coupled systems, electronic coherence effects would be minimal. Usually, the electronic coherence decays rather quickly, in 100–200 fs, and thus bares no influence for energy transfer dynamics on longer timescales. Their relationship with ultrafast energy transfer, however, remains a widely contested issue to this day, and thus falls outside the scope of the present review.

Constituents of photosynthetic systems (chlorophylls, carotenoids, etc.) have vibrational degrees of freedom, and vibrational coherence might also manifest as oscillations in 2D spectra. Vibrational contributions complicate the 2D maps due to transitions to and from vibrationally excited states, thus more peaks appear. Usually, vibrational coherence survives longer than electronic coherence, though the amplitude of the resulting oscillations is often limited by the relatively small Huang-Rhys factors in photosynthetic systems. In any case, the presence of all oscillations, whether electronic or vibrational, must be carefully taken into account when trying to extract information about the energy transfer dynamics from the 2D spectra. Note, however, that both types of coherence have been previously observed in pump–probe spectroscopy experiments [57,58].

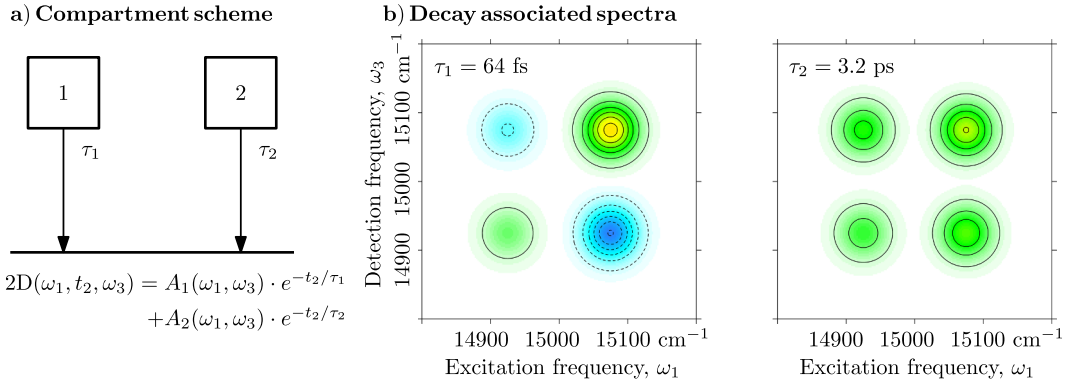

Fig. 11. Demonstration of DAS analysis of 2D spectra (data is the same as in Fig. 10). **a)** Chosen compartment scheme. **b)** Obtained DAS.

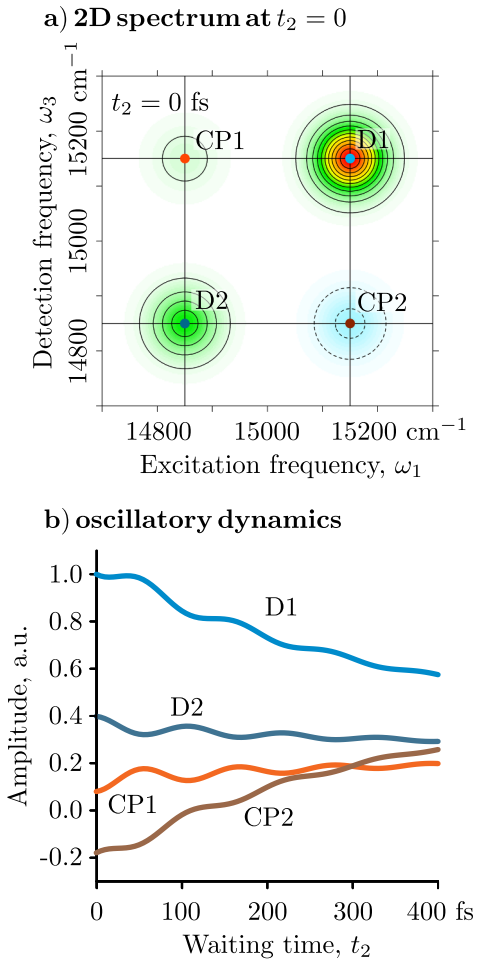

Fig. 12. Demonstration of oscillatory dynamics in 2D spectra. The system under consideration is a dimer similar to the one depicted in Fig. 8b, with energy gap between the excitonic states being set to 300 cm^{-1} and the downhill energy transfer rate being set to (400 fs)$^{-1}$. Coherent contributions, responsible for oscillatory signal, were assumed to decay with a time constant of 200 fs. **a)** 2D spectrum of the systems at zero waiting time, with diagonal peaks and cross-peaks marked by colored dots. **b)** Dynamics of the selected peaks, line color matches the color of dots in **a)**. (For interpretation of the references to color in this figure legend, the reader is referred to the web version of this article.)

4. Discussion

Now let us briefly discuss several applications of 2D spectroscopy, where important and interesting results were obtained. One of the foremost and well-known examples was 2D spectroscopy experiment employed on Fenna–Matthews–Olson (FMO) protein complex from green sulphur bacteria [14]. 2D spectra corresponding to 77 K revealed the dynamics of the peaks and allowed the authors to determine the energy transfer cascade. Recent experimental work on FMO was described in Ref. [59] and the improvements in the temporal and spectral resolutions permitted the authors to propose an updated energy relaxation scheme.

A very impressive piece of work was presented in Ref. [24], where 2D spectroscopy was used to map the energy relaxation cascade in the whole photosynthetic system of green sulphur bacteria, from the chlorosome through the FMO complex to the reaction center (RC). The 2D spectra presented therein covered a spectral range over 100 nm, and detailed information could be extracted about the energy levels and the peak structure. The same single experiment provided information about the energy transfer timescales from hundreds of femtoseconds to hundreds of picoseconds. The FMO was found to be an energy conduit from the chlorosome to the RC.

High time resolution of the 2D spectroscopy experiments was instrumental in several cases to obtain results that were not discovered in previous spectroscopic measurements. In Ref. [60], a sub-100 fs energy relaxation timescale was determined in the major light-harvesting complex from higher plants (LHCII). An ultrafast energy transfer with timescale of 60 fs from chlorophyll *c* to chlorophyll *a* molecules was observed in the fucoxanthin-chlorophyll protein complex [46]. Such timescale was inferred, but never directly measured in previous pump–probe measurements. Additionally, ultrafast energy relaxation on the order of 50 fs in Photosystem I was also obtained from 2D spectroscopy experiments [20,61].

We would also like to note some results obtained from the 2D spectroscopy on the photosynthetic RCs. In Ref. [17], 2D spectra of the Photosystem II RC was presented, whose analysis revealed the dominant timescales of energy and charge transfer. These timescales were also observed to possess inhomogeneity in the spectral range of the excitonic manifold. More recently, 2D spectra of the bacterial RC was presented in Ref. [62] and a detailed charge separation pathway model was constructed from its analysis.

In this paper, we kept the discussion on oscillatory features in the 2D spectra, together with description of electronic, vibrational (or possibly vibronic) coherence, to a minimum. This is because the oscillations in 2D spectroscopy have too often overshadowed the considerably more important results, concerning the timescales and pathways of energy or charge transfer. Nevertheless, we list several references on this issue, that an interested reader might wish to consult [15,22, 23, 63-73], where issues from experimental observations of coherence and the analysis of experimental data to its theoretical description are given.

5. Conclusions and outlook

Despite inherent complexities of both the experimental setup and theoretical description, the main ideas of 2D spectroscopy are relatively straightforward. This review article tried to highlight many parallels between the 2D and pump–probe spectroscopies to help the readers place the former in a proper context. We hope that this paper will prove to be helpful for the researchers in photosynthesis.

It is perhaps worthwhile to reiterate the key strengths of 2D spectroscopy. First, the uncoupling of time and excitation frequency resolution allows the researchers to follow the dynamics of specific states with selective excitation and excellent time resolution. Second, lack of background signals means that great signal-to-noise ratio can be achieved. Third, a single run of 2D spectroscopy experiment provides information along a wide range of excitation frequency axis, while using pump–probe technique many separate measurements with differing excitation frequency are needed.

For the last fifteen years, 2D spectroscopy contributed heavily to our understanding of excitation dynamics in photosynthetic molecular complexes. It is a safe bet that it will continue to do so for a foreseeable future. Therefore the fundamental understanding of this approach and of its information content will become more and more unavoidable, even for biologically-oriented researchers. Knowledge of the basic principles is also a prerequisite to appreciate the developments that are currently in progress. In particular, we would like to mention the development of 2D electronic Stark spectroscopy [74], which should provide new and exciting information about the charge transfer states in photosynthetic light-harvesting complexes and RCs. 2D spectroscopy thus still has a lot to provide for the science of photosynthesis.

Transparency document

The Transparency document associated with this article can be found, in online version.

Acknowledgments

We would like to thank all our coauthors on papers on 2D spectroscopy.

References

[1] R. Croce, H. van Amerongen, Natural strategies for photosynthetic light harvesting, Nat. Chem. Biol. 10 (2014) 492–501.
[2] R.E. Blankenship, Molecular Mechanisms of Photosynthesis, 2nd Ed., Wiley Blackwell, Chichester, 2014.
[3] J. Deisenhofer, O. Epp, K. Miki, R. Huber, H. Michel, X-ray structure analysis of a membrane protein complex, J. Mol. Biol. 180 (2) (1984) 385–398.
[4] A.V. Ruban, The Photosynthetic Membrane: Molecular Mechanisms and Biophysics of Light Harvesting, Wiley, Chichester, 2013.
[5] M. Pope, C.E. Swenberg, Electron Processes in Organic Crystals, Oxford University Press, New York/Oxford, 1999.
[6] H. van Amerongen, L. Valkunas, R. van Grondelle, Photosynthetic Excitons, World Scientific, Singapore, 2000.
[7] M.G. Rockley, M.W. Windsor, R.J. Cogdell, W.W. Parson, Picosecond detection of an intermediate in the photochemical reaction of bacterial photosynthesis, Proc. Natl. Acad. Sci. U. S. A. 72 (6) (1975) 2251–2255.
[8] D. Holten, M.W. Windsor, Picosecond flash photolysis in biology and biophysics, Annu. Rev. Biophys. Bioeng. 7 (1) (1978) 189–227.
[9] V. Shuvalov, A. Klevanik, A. Sharkov, P. Kryukov, K. Bacon, Picosecond spectroscopy of photosystem I reaction centers, FEBS Lett. 107 (2) (1979) 313–316.
[10] N.W. Woodbury, M. Becker, D. Middendorf, W.W. Parson, Picosecond kinetics of the initial photochemical electron-transfer reaction in bacterial photosynthetic reaction centers, Biochemistry 24 (26) (1985) 7516–7521.
[11] M.R. Wasielewski, D.G. Johnson, M. Seibert, Govindjee, Determination of the primary charge separation rate in isolated photosystem II reaction centers with 500-fs time resolution, Proc. Natl. Acad. Sci. U. S. A. 86 (2) (1989) 524–528.
[12] S. Hess, M. Chachisvilis, K. Timpmann, M.R. Jones, G.J. Fowler, C.N. Hunter, V. Sundström, Temporally and spectrally resolved subpicosecond energy transfer within the peripheral antenna complex (LH2) and from LH2 to the core antenna complex in photosynthetic purple bacteria, Proc. Natl. Acad. Sci. U. S. A. 92 (26) (1995) 12333–12337.
[13] D.M. Jonas, Two-dimensional femtosecond spectroscopy, Annu. Rev. Phys. Chem. 54 (2003) 425–463.
[14] T. Brixner, J. Stenger, H.M. Vaswani, M. Cho, R.E. Blankenship, G.R. Fleming, Two-dimensional spectroscopy of electronic couplings in photosynthesis, Nature 434 (2005) 625–628.
[15] G.S. Engel, T.R. Calhoun, E.L. Read, T.K. Ahn, T. Mančal, Y.C. Cheng, R.E. Blankenship, G.R. Fleming, Evidence for wavelike energy transfer through quantum coherence in photosynthetic systems, Nature 446 (2007) 782–786.
[16] E.L. Read, G.S. Schlau-Cohen, G.S. Engel, J. Wen, R.E. Blankenship, G.R. Fleming, Visualization of excitonic structure in the Fenna-Matthews-Olson photosynthetic complex by polarization-dependent two-dimensional electronic spectroscopy, Biophys. J. 95 (2008) 847–856.
[17] J.A. Myers, K.L.M. Lewis, F.D. Fuller, P.F. Tekavec, C.F. Yocum, J.P. Ogilvie, Two-dimensional electronic spectroscopy of the D1-D2-cyt b559 photosystem II reaction center complex, J. Phys. Chem. Lett. 1 (19) (2010) 2774–2780.
[18] J. Dostál, T. Mančal, R. Augulis, F. Vácha, J. Pšenčik, D. Zigmantas, Two-dimensional electronic spectroscopy reveals ultrafast energy diffusion in chlorosomes, J. Am. Chem. Soc. 134 (28) (2012) 11611–11617.
[19] E. Harel, G.S. Engel, Quantum coherence spectroscopy reveals complex dynamics in bacterial light-harvesting complex 2 (LH2), Proc. Natl. Acad. Sci. U. S. A. 109 (3) (2012) 706–711.
[20] J.M. Anna, E.E. Ostroumov, K. Maghlaoui, J. Barber, G.D. Scholes, Two-dimensional electronic spectroscopy reveals ultrafast downhill energy transfer in photosystem I trimers of the cyanobacterium *Thermosynechococcus elongatus*, J. Phys. Chem. Lett. 3 (24) (2012) 3677–3684.
[21] G.S. Schlau-Cohen, A. Ishizaki, T.R. Calhoun, N.S. Ginsberg, M. Ballottari, R. Bassi, G.R. Fleming, Elucidation of the timescales and origins of quantum electronic coherence in LHCII, Nat. Chem. 4 (2012) 389–395.
[22] E. Romero, R. Augulis, V.I. Novoderezhkin, M. Ferretti, J. Thieme, D. Zigmantas, R.V. Grondelle, Quantum coherence in photosynthesis for efficient solar-energy conversion, Nat. Phys. 10 (2014) 676–682.
[23] F.D. Fuller, J. Pan, A. Gelzinis, V. Butkus, S.S. Senlik, D.E. Wilcox, C.F. Yocum, L. Valkunas, D. Abramavicius, J.P. Ogilvie, Vibronic coherence in oxygenic photosynthesis, Nat. Chem. 6 (2014) 706–711.
[24] J. Dostál, J. Pšenčik, D. Zigmantas, *In situ* mapping of the energy flow through the entire photosynthetic apparatus, Nat. Chem. 8 (2016) 705–710.
[25] J. Pan, A. Gelzinis, V. Chorosajev, M. Vengris, S.S. Senlik, J.-R. Shen, L. Valkunas, D. Abramavicius, J.P. Ogilvie, Ultrafast energy transfer within the photosystem II core complex, Phys. Chem. Chem. Phys. 19 (2017) 15356–15367.
[26] P.D. Dahlberg, P.-C. Ting, S.C. Massey, M.A. Allodi, E.C. Martin, C.N. Hunter, G.S. Engel, Mapping the ultrafast flow of harvested solar energy in living photosynthetic cells, Nat. Commun. 8 (2017) 998.
[27] M. Cho, Coherent Two-dimensional optical spectroscopy, Chem. Rev. 108 (4) (2008) 1331–1418.
[28] D. Abramavicius, B. Palmieri, D.V. Voronine, F. Šanda, S. Mukamel, Coherent multidimensional optical spectroscopy of excitons in molecular aggregates; quasiparticle versus supermolecule perspectives, Chem. Rev. 109 (2009) 2350–2408.
[29] V. Butkus, D. Abramavicius, A. Gelzinis, L. Valkunas, Two-dimensional optical spectroscopy of molecular aggregates, Lith. J. Phys. 50 (2010) 267–303.
[30] G.S. Schlau-Cohen, A. Ishizaki, G.R. Fleming, Two-dimensional electronic spectroscopy and photosynthesis: fundamentals and applications to photosynthetic light-harvesting, Chem. Phys. 386 (1-3) (2011) 1–22.
[31] A.M. Brańczyk, D.B. Turner, G.D. Scholes, Crossing disciplines — a view on two-dimensional optical spectroscopy, Ann. Phys. 526 (1-2) (2014) 31–49.
[32] F.D. Fuller, J.P. Ogilvie, Experimental implementations of two-dimensional Fourier transform electronic spectroscopy, Annu. Rev. Phys. Chem. 66 (1) (2015) 667–690.
[33] J.O. Tollerud, J.A. Davis, Coherent multi-dimensional spectroscopy: experimental considerations, direct comparisons and new capabilities, Prog. Quantum Electron. 55 (2017) 1–34.
[34] H. Li, S.T. Cundiff, Chapter one — 2D coherent spectroscopy of electronic transitions, Advances In Atomic, Molecular, and Optical Physics, vol. 66, Academic Press, 2017, pp. 1–48.
[35] S. Mukamel, Principles of Nonlinear Optical Spectroscopy, Oxford University Press, New York, 1995.
[36] M. Cho, Two-dimensional Optical Spectroscopy, CRC Press, Boca Raton, 2009.
[37] P. Hamm, M. Zanni, Concepts and Methods of 2D Infrared Spectroscopy, Cambridge University Press, New York, 2011.
[38] L. Valkunas, D. Abramavicius, T. Mančal, Molecular Excitation Dynamics and Relaxation: Quantum Theory and Spectroscopy, Wiley-VCH, Berlin, 2013.
[39] J.A. Myers, K.L. Lewis, P.F. Tekavec, J.P. Ogilvie, Two-color two-dimensional Fourier transform electronic spectroscopy with a pulse-shaper, Opt. Express 16 (22) (2008) 17420–17428.
[40] R. Moca, S.R. Meech, I.A. Heisler, Two-dimensional electronic spectroscopy of chlorophyll a: solvent dependent spectral evolution, J. Phys. Chem. B 119 (27) (2015) 8623–8630.
[41] D. Brida, C. Manzoni, G. Cerullo, Phase-locked pulses for two-dimensional spectroscopy by a birefringent delay line, Opt. Lett. 37 (15) (2012) 3027–3029.
[42] H. Zheng, J.R. Caram, P.D. Dahlberg, B.S. Rolczynski, S. Viswanathan, D.S. Dolzhnikov, A. Khadivi, D.V. Talapin, G.S. Engel, Dispersion-free continuum two-dimensional electronic spectrometer, Appl. Opt. 53 (9) (2014) 1909–1917.
[43] V. Butkus, A. Gelzinis, R. Augulis, A. Gall, C. Büchel, B. Robert, D. Zigmantas, L. Valkunas, D. Abramavicius, Coherence and population dynamics of chlorophyll excitations in FCP complex: two-dimensional spectroscopy study, J. Chem. Phys. 142 (21) (2015) 212414.
[44] C. Consani, G. Auböck, F. van Mourik, M. Chergui, Ultrafast tryptophan-to-heme electron transfer in myoglobins revealed by UV 2D spectroscopy, Science 339 (2013) 1586–1589.
[45] M. Reinhard, G. AubÃűck, N.A. Besley, I.P. Clark, G.M. Greetham, M.W.D. Hanson-Heine, R. Horvath, T.S. Murphy, T.J. Penfold, M. Towrie, M.W. George, M. Chergui, Photoaquation mechanism of hexacyanoferrate(II) ions: ultrafast 2D UV and transient visible and IR spectroscopies, J. Am. Chem. Soc. 139 (21) (2017) 7335–7347.
[46] E. Songaila, R. Augulis, A. Gelzinis, V. Butkus, A. Gall, C. Büchel, B. Robert, D. Zigmantas, D. Abramavicius, L. Valkunas, Ultrafast energy transfer from chlorophyll c_2 to chlorophyll *a* in fucoxanthin-chlorophyll protein complex, J. Phys. Chem. Lett. 4 (21) (2013) 3590–3595.
[47] A. Gelzinis, V. Butkus, E. Songaila, R. Augulis, A. Gall, C. Büchel, B. Robert, D. Abramavicius, D. Zigmantas, L. Valkunas, Mapping energy transfer channels in fucoxanthin-chlorophyll protein complex, Biochim. Biophys. Acta 1847 (2) (2015) 241–247.
[48] M. Maiuri, J. Réhault, A.-M. Carey, K. Hacking, M. Garavelli, L. Lüer, D. Polli, R.J. Cogdell, G. Cerullo, Ultra-broadband 2D electronic spectroscopy of carotenoid-bacteriochlorophyll interactions in the LH1 complex of a purple bacterium, J. Chem. Phys. 142 (21) (2015) 212433.
[49] A. Konar, R. Sechrist, Y. Song, V.R. Policht, P.D. Laible, D.F. Bocian, D. Holten, C. Kirmaier, J.P. Ogilvie, Electronic interactions in the bacterial reaction center revealed by two-color 2D electronic spectroscopy, J. Phys. Chem. Lett. 9 (18) (2018) 5219–5225.
[50] D. Abramavicius, V. Butkus, J. Bujokas, L. Valkunas, Manipulation of two-dimensional spectra of excitonically coupled molecules by narrow-bandwidth laser pulses, Chem. Phys. 372 (1-3) (2010) 22–32.
[51] E.E. Ostroumov, R.M. Mulvaney, J.M. Anna, R.J. Cogdell, G.D. Scholes, Energy transfer pathways in light-harvesting complexes of purple bacteria as revealed by global kinetic analysis of two-dimensional transient spectra, J. Phys. Chem. B 117 (38) (2013) 11349–11362.
[52] J. Alster, H. Lokstein, J. Dostál, A. Uchida, D. Zigmantas, 2D spectroscopy study of water-soluble chlorophyll-binding protein from *Lepidium virginicum*, J. Phys. Chem. B 118 (13) (2014) 3524–3531.
[53] V.I. Prokhorenko, Global Analysis of Multi-dimensional experimental data, Eur. Photochem. Assoc. Newsletter, 2012, pp. 21–23 June.
[54] I.H. van Stokkum, D.S. Larsen, R. van Grondelle, Global and target analysis of time-resolved spectra, Biochim. Biophys. Acta 1657 (2-3) (2004) 82–104.
[55] A. Volpato, L. Bolzonello, E. Meneghin, E. Collini, Global analysis of coherence and population dynamics in 2D electronic spectroscopy, Opt. Express 24 (21) (2016) 24773–24785.
[56] J. Dostál, B. Beneŏvá, T. Brixner, Two-dimensional electronic spectroscopy can fully characterize the population transfer in molecular systems, J. Chem. Phys. 145 (12) (2016) 124312.
[57] M.H. Vos, J.C. Lambry, S.J. Robles, D.C. Youvan, J. Breton, J.L. Martin, Direct observation of vibrational coherence in bacterial reaction centers using femtosecond absorption spectroscopy. Proc. Natl. Acad. Sci. U. S. A. 88 (20) (1991) 8885–8889.
[58] S. Savikhin, D.R. Buck, W.S. Struve, Oscillating anisotropies in a bacteriochlorophyll protein: evidence for quantum beating between exciton levels, Chem.

Phys. 223 (2) (1997) 303–312.
[59] E. Thyrhaug, K. židek, J. Dostál, D. Bína, D. Zigmantas, Exciton structure and energy transfer in the Fenna-Matthews-Olson complex, J. Phys. Chem. Lett. 7 (2016) 1653–1660.
[60] G.S. Schlau-Cohen, T.R. Calhoun, N.S. Ginsberg, E.L. Read, M. Ballottari, R. Bassi, R. van Grondelle, G.R. Fleming, Pathways of energy flow in LHCII from two-dimensional electronic spectroscopy, J. Phys. Chem. B 113 (46) (2009) 15352–15363.
[61] Y. Lee, M. Gorka, J.H. Golbeck, J.M. Anna, Ultrafast energy transfer involving the red chlorophylls of cyanobacterial photosystem I probed through two-dimensional electronic spectroscopy, J. Am. Chem. Soc. 140 (37) (2018) 11631–11638.
[62] A. Niedringhaus, V.R. Policht, R. Sechrist, A. Konar, P.D. Laible, D.F. Bocian, D. Holten, C. Kirmaier, J.P. Ogilvie, Primary processes in the bacterial reaction center probed by two-dimensional electronic spectroscopy, Proc. Natl. Acad. Sci. U. S. A. 115 (14) (2018) 3563–3568.
[63] G. Panitchayangkoon, D. Hayes, K.A. Fransted, J.R. Caram, E. Harel, J. Wen, R.E. Blankenship, G.S. Engel, Long-lived quantum coherence in photosynthetic complexes at physiological temperature, Proc. Natl. Acad. Sci. U. S. A. 107 (29) (2010) 12766–12770.
[64] E. Collini, C.Y. Wong, K.E. Wilk, P.M.G. Curmi, P. Brumer, G.D. Scholes, Coherently wired light-harvesting in photosynthetic marine algae at ambient temperature, Nature 463 (2010) 644–647.
[65] V. Butkus, D. Zigmantas, L. Valkunas, D. Abramavicius, Vibrational vs. electronic coherences in 2D spectrum of molecular systems, Chem. Phys. Lett. 545 (2012) 40–43.
[66] S. Westenhoff, D. Paleček, P. Edlund, P. Smith, D. Zigmantas, Coherent picosecond exciton dynamics in a photosynthetic reaction center, J. Am. Chem. Soc. 134 (40) (2012) 16484–16487.
[67] T. Mančal, N. Christensson, V. Lukeš, F. Milota, O. Bixner, H.F. Kauffmann, J. Hauer, System-dependent signatures of electronic and vibrational coherences in electronic two-dimensional spectra, J. Phys. Chem. Lett. 3 (11) (2012) 1497–1502.
[68] V. Butkus, D. Zigmantas, D. Abramavicius, L. Valkunas, Distinctive character of electronic and vibrational coherences in disordered molecular aggregates, Chem. Phys. Lett. 587 (2013) 93–98.
[69] V. Tiwari, W.K. Peters, D.M. Jonas, Electronic resonance with anticorrelated pigment vibrations drives photosynthetic energy transfer outside the adiabatic framework, Proc. Natl. Acad. Sci. U. S. A. 110 (4) (2013) 1203–1208.
[70] A. Halpin, P.J.M. Johnson, R. Tempelaar, R.S. Murphy, J. Knoester, T.L.C. Jansen, R.J.D. Miller, Two-dimensional spectroscopy of a molecular dimer unveils the effects of vibronic coupling on exciton coherences, Nat. Chem. 6 (2014) 196–201.
[71] V. Butkus, L. Valkunas, D. Abramavicius, Vibronic phenomena and exciton-vibrational interference in two-dimensional spectra of molecular aggregates, J. Chem. Phys. 140 (3) (2014) 034306.
[72] V. Butkus, J. Alster, E. Bašinskaitė, R. Augulis, P. Neuhaus, L. Valkunas, H.L. Anderson, D. Abramavicius, D. Zigmantas, Discrimination of diverse coherences allows identification of electronic transitions of a molecular nanoring, J. Phys. Chem. Lett. 8 (10) (2017) 2344–2349.
[73] F.V. de A Camargo, L. Grimmelsmann, H.L. Anderson, S.R. Meech, I.A. Heisler, Resolving vibrational from electronic coherences in two-dimensional electronic spectroscopy: the role of the laser spectrum, Phys. Rev. Lett. 118 (2017) 033001.
[74] A. Loukianov, A. Niedringhaus, B. Berg, J. Pan, S.S. Senlik, J.P. Ogilvie, Two-dimensional electronic Stark spectroscopy, J. Phys. Chem. Lett. 8 (3) (2017) 679–683.